Biochemistry

 Volume 37, Number 39 September 29, 1998

Accelerated Publications

Crystal Structure of Tyrosine Hydroxylase with Bound Cofactor Analogue and Iron at 2.3 Å Resolution: Self-Hydroxylation of Phe300 and the Pterin-Binding Site[†,‡]

Kenneth E. Goodwill,[§] Christelle Sabatier, and Raymond C. Stevens*

Department of Chemistry, University of California, Berkeley, California 94720

Received June 19, 1998; Revised Manuscript Received August 10, 1998

ABSTRACT: TyrOH is a non-heme iron enzyme which uses molecular oxygen to hydroxylate tyrosine to form L-dihydroxyphenylalanine (L-DOPA), and tetrahydrobiopterin to form 4a-hydroxybiopterin, in the rate-limiting step of the catecholamine biosynthetic pathway. The 2.3 Å crystal structure of the catalytic and tetramerization domains of rat tyrosine hydroxylase (TyrOH) in the presence of the cofactor analogue 7,8-dihydrobiopterin and iron shows the mode of pterin binding and the proximity of its hydroxylated 4a carbon to the required iron. The pterin binds on one face of the large active-site cleft, forming an aromatic π-stacking interaction with Phe300. This phenylalanine residue of TyrOH is found to be hydroxylated in the meta position, most likely through an autocatalytic process, and to consequently form a hydrogen bond to the main-chain carbonyl of Gln310 which anchors Phe300 in the active site. The bound pterin forms hydrogen bonds from N-8 to the main-chain carbonyl of Leu295, from O-4 to Tyr371 and Glu376, from the C-1′ OH to the main-chain amides of Leu294 and Leu295, and from the C-2′ hydroxyl to an iron-coordinating water. The part of the pterin closest to the iron is the O-4 carbonyl oxygen at a distance of 3.6 Å. The iron is 5.6 Å from the pterin 4a carbon which is hydroxylated in the enzymatic reaction. No structural changes are observed between the pterin bound and the nonliganded enzyme. On the basis of these structures, molecular oxygen could bind in a bridging position optimally between the pterin C-4a and iron atom prior to substrate hydroxylation. This structure represents the first report of close interactions between pterin and iron in an enzyme active site.

Tyrosine hydroxylase (TyrOH, EC 1.14.16.2) catalyzes the conversion of tyrosine to L-dihydroxyphenylalanine (L-DOPA), the rate-limiting step in the biosynthesis of the catecholamines dopamine, noradrenaline, and adrenaline (*1*). The enzyme requires a non-heme ferrous iron atom and stoichiometric amounts of tetrahydrobiopterin for activity. The pterin is a dissociable substrate of TyrOH, as opposed to the tightly bound pterin observed in nitric oxide synthase (*2*). The hydroxylated pterin product is recycled through dehydration by 4a-carbinolamine dehydratase (DCoH, EC 4.2.1.96) and reduction by dihydropteridine reductase (DHPR, EC 1.6.99.7) as shown in Scheme 1. Molecular oxygen is the third substrate of TyrOH, providing the source of oxygen for both the hydroxylation of tyrosine and the accompanying

[†] For K.E.G., part of this work was done during the tenure of a predoctoral fellowship from the American Heart Association, California affiliate. Financial support for this research was provided by the Keck Foundation, an NSF Young Investigator Award, and the LBL Physical Biosciences Division.

[‡] The coordinates have been deposited with the Brookhaven Protein Data Bank, accession number 2TOH.

* To whom correspondence should be addressed. E-mail: stevens@adrenaline.berkeley.edu.

[§] Present address: UCLA-DOE Laboratory of Structural Biology and Molecular Medicine, Molecular Biology Institute, University of California, Los Angeles, CA 90095.

S0006-2960(98)01462-7 CCC: $15.00
Published on Web 09/29/1998

Scheme 1: Regeneration Cycle of the Pterin Substrate Used by TyrOH[a]

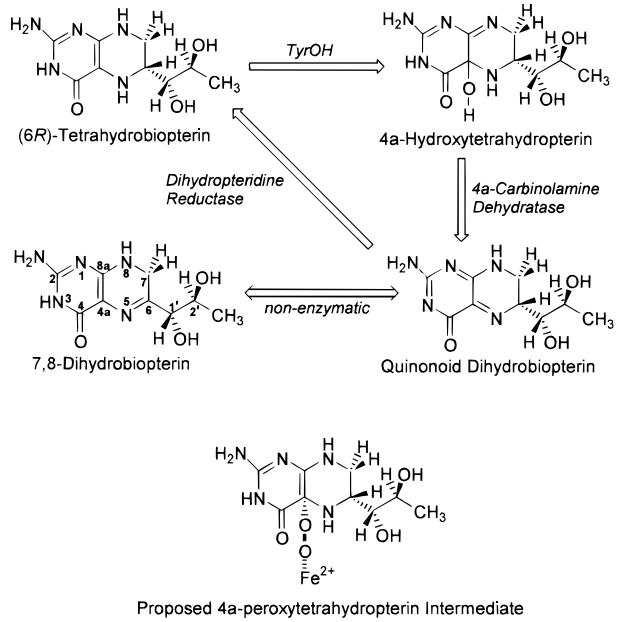

[a] The numbering given for 7,8-dihydrobiopterin is the convention used in this paper. the structure of a possible 4a-peroxytetrahydropterin intermediate is shown below the cycle.

oxidation of tetrahydrobiopterin to 4a-hydroxybiopterin.

TyrOH is expressed in the adrenal medulla and the catecholinergic neurons of the central and peripheral nervous systems (*3*). TyrOH is a member of the highly homologous pterin-dependent aromatic amino acid hydroxylase family which also includes phenylalanine hydroxylase (PheOH, EC 1.14.16.1) and tryptophan hydroxylase (TrpOH, EC 1.14.16.4) (*3*). These enzymes are intimately associated with neuronal function through their catalysis of the rate-limiting step in the pathways for catecholamine biosynthesis, phenylalanine catabolism, and serotonin biosynthesis, respectively. All three of the aromatic amino acid hydroxylases utilize a nonheme iron and molecular oxygen to simultaneously hydroxylate their respective amino acid substrates and a tetrahydrobiopterin cosubstrate (*3*). The enzymes from eukaryotic sources share a three domain structure. There is an N-terminal regulatory domain of 100−170 residues, which has a pairwise homology of about 25%. This is followed by a 270 residue catalytic domain exhibiting 80% sequence homology and a 65% pairwise sequence identity. The C-terminal 40 residues in the family form a tetramerization domain with a 60% pairwise homology. Bacterial versions of PheOH have been reported from *Chromobacterium violaceum (4*) and *Pseudomonas aeroginosa (5*) which lack both the regulatory and tetramerization domains. Deletion experiments with the eukaryotic enzymes have demonstrated that the highly conserved catalytic domain can promote the reaction independently of the other domains *(3*).

The reactions catalyzed by these three enzymes are extremely similar (*3*). In particular, TyrOH and PheOH have been well characterized due to the availability of stable recombinant enzyme. Eukaryotic versions of these enzymes have been shown to utilize ferrous iron. Substitution of iron with other divalent metals results in the loss of catalytic activity. Both enzymes show a spontaneous autooxidation in vitro of the ferrous iron to a ferric state. The ferric state is strongly inhibited by catechol complexes which can form from the downstream products of TyrOH. A stoichiometric reaction of tetrahydrobiopterin with the ferric enzyme to produce the ferrous form and to displace bound catechols has been demonstrated in vitro (*6*−*8*). One possible role of tetrahydrobiopterin in vivo, in addition to its role in normal enzyme turnover, may be to return the ferric enzyme to the active ferrous state.

The reactions of TyrOH and PheOH have been studied by steady-state kinetics, partitioning effects of substrate substitution, and kinetic isotope effects (*3*, *9*−*11*). Steady-state kinetic analysis of TyrOH has shown that this reaction proceeds by an ordered binding of pterin, oxygen, and then amino acid substrate (*9*). No reaction occurs until all three substrates are bound. The rate-limiting step appears to be the slow formation of a hydroxylating intermediate which can either react rapidly with the amino acid substrate or break down nonproductively. ^{18}O isotope effect studies have suggested that the rate-limiting step is the reaction of oxygen with the pterin, and not with the iron (*11*). A pterin peroxide species has been proposed as the reactive intermediate (Scheme 1) (*3*, *10*−*12*).

Structures have been determined for the iron-bound forms of rat TyrOH (*13*) and human PheOH (*14*, *15*). Both enzymes show an iron coordination of two histidines, a glutamate, and two or three water molecules. The locations of the iron ligands are similar in the two structures, with PheOH containing an additional water which is not observed in TyrOH. The catalytic domain of this enzyme family shows no sequence or structure homology to other proteins. Therefore, to probe the nature of the pterin cosubstrate binding site and determine its proximity to the active-site iron, the structure of a binary complex of TyrOH cocrystallized with iron and 7,8-dihydrobiopterin has been solved to 2.3 Å resolution. The latter is a substrate analogue which has been shown to bind competitively with the tetrahydrobiopterin substrate and which is significantly more stable than tetrahydrobiopterin. The K_m for tetrahydrobiopterin has been found to be 15−30 μM (*1*), and the K_i of 7,8-dihydrobiopterin versus tetrahydrobiopterin has been found to be 70 μM (*16*).

EXPERIMENTAL PROCEDURES

Crystallization and Data Collection. DNA coding for the catalytic and tetramerization domains of rat tyrosine hydroxylase was expressed and purified from *Escherichia coli* as previously described (*13*). Cocrystals of the binary complex with iron and 7,8-dihydrobiopterin were obtained by equilibrium dialysis. All crystal growth experiments were conducted with solutions degassed by helium and in a sealed chamber under positive nitrogen gas pressure held at 4 °C. The protein was concentrated to 16 mg/mL (0.4 mM protein, twice the concentration used for the ligand-free crystals) and incubated with 4 mM ferrous ammonium sulfate prior to setting up the dialysis buttons. The solution outside the dialysis membrane contained 1.15 M ammonium sulfate, 3.2% PEG 200, 5% glycerol, 100 mM Tris, pH 7.9, and was saturated (3 mM) in 7,8-dihydrobiopterin (Schircks Laboratories, Jona, Switzerland). Crystals grew to 0.6 × 0.4 × 0.1 mm in 3 days under these crystallization conditions, which were the same as those used to grow the ligand-free crystals previously reported (*13*).

To avoid radiation-induced crystal decay, it was necessary to collect diffraction data from the crystals at 100 K. The cryoprotection solution consisted of the equilibrated crystallization solution with added glycerol and ammonium sulfate such that the final glycerol concentration was 25% and the final ammonium sulfate concentration remained 1.15 M. The crystal was equilibrated via a two step serial transfer over the course of 20 min. Data were collected at the Stanford Synchrotron Radiation Laboratory beamline 7-1 using 1.08 Å wavelength radiation, with a MAR detector (MAR Research). The data were processed with DENZO and SCALEPACK (*17*). Programs from the CCP4 suite were used for various calculations (*18*). The binary complex crystallized in the space group *F*222 ($a = 189.5$ Å, $b = 148.6$ Å, $c = 57.0$ Å) with 1 monomer/asymmetric unit and a solvent content of 47%. These unit cell parameters were slightly different from those of the ligand-free form of the enzyme (*F*222, $a = 189.3$ Å, $b = 148.3$ Å, $c = 58.0$ Å).

Model Building and Refinement. The iron-bound TyrOH structure was used as an initial starting model (*13*). The program CNS (*19*) was used for the structure refinement. O was used for atomic model building (*20*). Rigid body refinement was applied to the starting model with the tetramerization and catalytic domains defined as independent regions. This refinement resulted in a rigid body translation of the model along the *z*-axis and a drop in the *R*-factors from $R_{cryst} = 40.8\%$ and $R_{free} = 40.9\%$ to $R_{cryst} = 30.7\%$ and $R_{free} = 31.2\%$. Using an $|F_o - F_c|F_c$ electron density map after rigid body refinement, the 7,8-dihydrobiopterin could clearly be observed and was placed into the model. Composite simulated annealing omit maps, with spheres of either 7 or 10% of the atoms removed from the model, were used to guide manual rebuilding. These maps revealed additional residues not previously included in the original model (*13*); residues 160−162, 178−182, and 186−199. Several rounds of manual rebuilding were done, with each one followed by conjugate gradient minimization and restrained individual *B*-factor refinement. A maximum likelihood target was used in the refinement program. The final model for the binary complex includes residues 160−182 and 186−498, the active-site iron, one chloride ion, 7,8-dihydrobiopterin, and 178 water molecules. The Wilson *B*-factor for the X-ray diffraction data is 48.3, and the average *B*-factor for the refined model is 49.8. The average *B*-factor for the pterin (assuming full occupancy) is 83.6, and the iron *B*-factor is 41.0. This model refined to $R_{cryst} = 20.7\%$ and $R_{free} = 27.6\%$ using data from 40 to 2.3 Å, with a bulk solvent model and an anisotropic *B*-factor correction included (17 098 reflections having $F > 2\sigma F$, 94.1% of possible). The rmsd for bond lengths is 0.020 Å, and the rmsd for bond angles is 2.1°. The Ramachandran plot (*21*) shows that 90% of the residues are in the most favored regions, and none are in disallowed regions.

On the basis of improvements in the model made during refinement of the binary complex, the ligand-free model was reexamined. The model was modified to include residues 159−177 and 187−498, the active-site iron, one chloride ion, and 194 water molecules. With these improvements, the refinement statistics for this model went from previously reported values of $R_{cryst} = 22.4\%$ and $R_{free} = 29.0\%$ to $R_{cryst} = 21.3\%$ and $R_{free} = 26.2\%$ (data from 37 to 2.3 Å; 17 787 reflections having $F > 2\sigma F$, 96.6% of possible). A bulk solvent model and an anisotropic *B*-factor correction were included in the refinement. The rmsd for bond lengths is 0.019 Å, and the rmsd for bond angles is 2.0°. The Ramachandran plot shows that 93% of the residues are in the most favored regions, and none are in disallowed regions.

RESULTS AND DISCUSSION

The overall fold of TyrOH (Figure 1) has been described previously (*13*) and will only be briefly described here. The catalytic domain consists of residues 188−456 and forms a basket-like arrangement of primarily helices (49%) and loops (42%). The tetramerization domain consists of residues 457−498 and is formed by two β-strands and a 40 Å long α-helix. This helix contains a hydrophobic heptad repeat and forms a coiled coil at the core of the tetramer. The active site of TyrOH consists of a 17 Å deep cleft at the center of the catalytic domain basket. The cleft is lined primarily by four α-helices (residues 297−304, 329−340, 343−356, and 361−372). The opening into the active site consists of two loops (residues 423−428 and 290−296) that come to within 12 Å of each other as they reach over the top of the 30 Å wide active site.

The iron atom is 10 Å below the enzyme surface within the active-site cleft. The iron is directly coordinated by the "2-his-1-carboxylate facial triad", which has now been observed in the crystal structures of five different classes of non-heme iron proteins (*22*). These residues in TyrOH are His331 (N···Fe 2.1 Å), His336 (N···Fe 2.1 Å), and Glu376 (O···Fe 2.1 Å). Electron density is also observed for two water molecules at a distance of 2.0 Å from the iron. The coordination geometry is square pyramidal with His331 as the axial ligand and two water molecules joining the protein ligands in the equatorial positions. The iron atom is observed to be in the plane of the equatorial ligands.

Pterin-Binding Site. The residues near the iron of TyrOH are well conserved in the aromatic amino acid hydroxylase family. Three of these are hydrophobic residues which are completely conserved: Phe300, Phe309, and Pro327. Using the ligand-free structure (with rigid body refinement against the binary complex data) as the initial model, difference Fourier electron density maps ($|F_o - F_c|F_c$) using data from the binary complex crystals clearly showed electron density for the two nearly-flat heterocyclic rings of the pterin, π-stacked on Phe300. No other large continuous regions of electron density above 2.0σ were observed in the active site. The electron density also showed a narrow tail toward Glu332 which was subsequently modeled as the dihydroxypropyl chain at position C-6 of the pterin ring (Figures 2a and 3). Simulated annealing omit maps made during the course of the refinement showed excellent density for the amine attached to the carbon at position C-2 of the pterin ring, and a bound water molecule associated with that amine. Also, continuous electron density was observed from position C-4 of the pterin ring to the iron. The carbonyl oxygen at position 4 was modeled into this density. These three markers, at positions C-2, C-4, and C-6 of the pterin ring system, were used to determine the orientation of the bound 7,8-dihydrobiopterin.

The interatomic distances between Phe300 and the π-stacked pterin are about 3.5 Å (Figure 4). Similar aromatic π-stacking arrangements are seen with a phenylalanine in the

FIGURE 1: The TyrOH tetramer with each monomer drawn in a different color. The active site iron atoms are shown in red. This figure was prepared with MOLSCRIPT (*43*) and Raster3D (*44*).

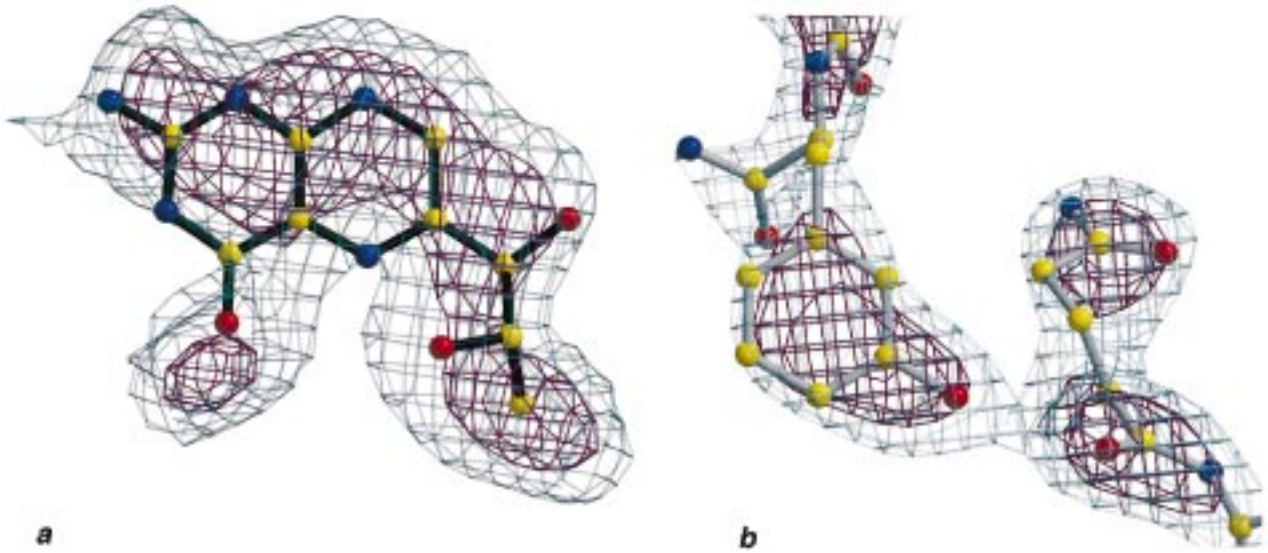

FIGURE 2: (a) Difference Fourier (omit) electron density ($|F_o - F_c|F_c$) for the 7,8-dihydropterin calculated using the final model. The light contour is at 1.6σ, and the darker contour is at 3.0σ. (b) Simulated annealing omit map electron density ($|F_o - F_c|F_c$) for the hydroxylated residue Phe300 and its hydrogen bond to the main chain carbonyl of Gln310. The light contour is at 2.0σ, and the darker contour is at 3.0σ. This figure was prepared with BOBSCRIPT (*45*).

structure of chicken dihydrofolate reductase (DHRF) complexed with biopterin (*23*) and with a tryptophan in the structure of nitric oxide synthase (NOS) with tetrahydrobiopterin bound (*2*). In the TyrOH complex, the pterin is about 10° offset from being parallel with the benzene ring of Phe300. In DHFR, this offset is about 37°. Several hydrogen bonds also contribute to pterin binding in TyrOH (Figure 4). N-8 of the pterin ring forms a hydrogen bond (3.1 Å, 120°) with the main-chain carbonyl of Leu295. The adjacent glycine at position 293 is conserved in all 14 known eukaryotic aromatic amino acid hydroxylases and most likely allows for flexibility in this loop region which is important for pterin binding (Figure 3). The carbonyl at position C-4 of the pterin ring forms two hydrogen bonds with active-site residues. One is with the iron-binding residue Glu376 (3.1 Å, 136°), and the second is with the highly conserved residue Tyr371 (3.2 Å, 98°). Three additional hydrogen bonds are formed by the hydroxypropyl group attached to C-6, although the electron density indicates that there is a degree of flexibility in this portion of the pterin. The hydroxyl at position C-1′ forms a hydrogen bond with the main-chain amides of residues Leu294 (3.2 Å, 85°) and Leu

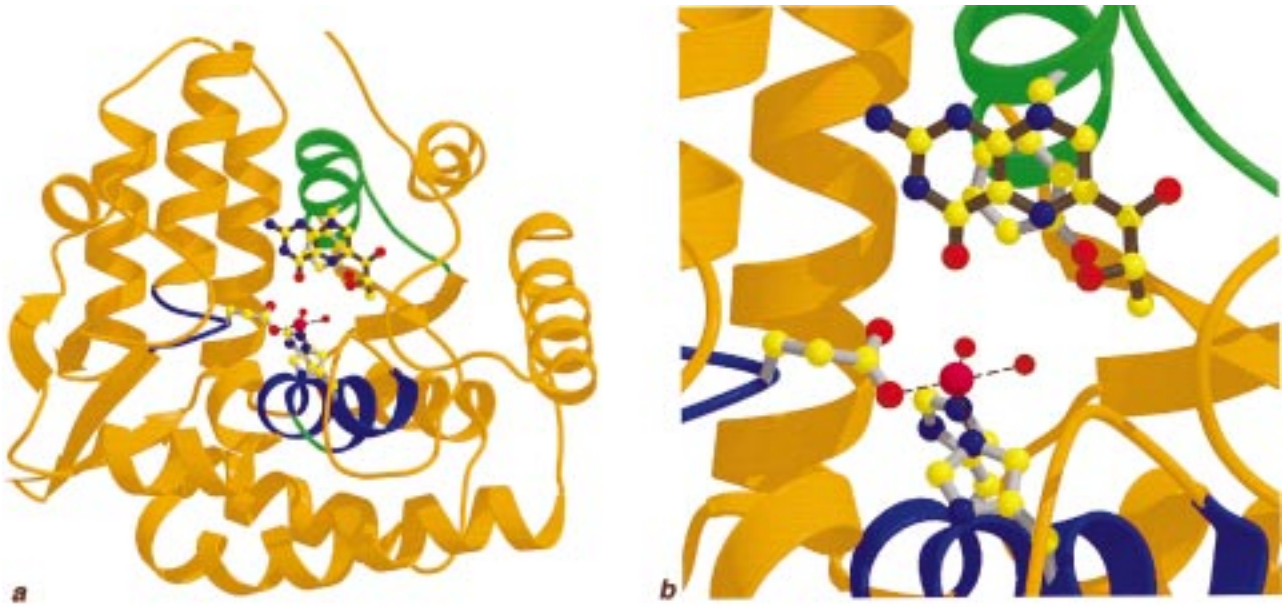

FIGURE 3: (a) A view looking directly into the active site cleft of the catalytic domain. The three iron coordinating residues (His331, His336, and Glu376) are shown in ball-and-stick format, as is the hydroxylated Phe300 which is behind the pterin. The coordination of the three residues and two waters to the iron is represented with dashed lines. The secondary structure portions containing the iron coordinating residues are shown in blue, and the glycine which accommodates a kink in the His331 and His336 helix is shown in green. The helix which contains Phe300 and the adjacent loop region which participates in pterin binding is also shown in green. (b) A closer view of the pterin binding site in panel a.

295 (3.2 Å, 125°), and the hydroxyl at C-2′ forms a hydrogen bond with an iron-coordinating water (3.3 Å). This hydroxyl is also 4.0 Å from the carboxyl of the conserved residue Glu332.

The pterin-bound and ligand-free structures are isomorphous with an rmsd of 0.18 Å, well within the experimental error. No major conformational changes are observed between the two structures. Seven waters which are observed in the active site of the TyrOH ligand-free structure are displaced upon pterin binding. The two waters which are coordinated to the iron in the ligand-free structure are unchanged in the binary complex. In both structures, the iron atom lies in the plane formed by the ligands His336, Glu376, and H_2Os 601 and 602 (Figure 3). His331 forms the axial ligand to complete the square pyramidal geometry. In PheOH (*14*), a third water molecule opposite His331 completes an octahedral geometry. Water binding at this same position in TyrOH appears to be blocked due to a slightly different position of Glu376 in the two structures. However, the ligand-free TyrOH structure shows density for a water molecule 3.1 Å away from the iron in this axial position. That water is displaced upon pterin binding by the carbonyl oxygen at the C-4 position. This oxygen, at a distance of 3.6 Å, is the closest contact between the pterin and the iron.

Meta Hydroxylation of Phe300. Difference Fourier electron density maps ($|F_o - F_c|F_c$) for the binary complex consistently showed a peak of electron density at a distance of 1.4 Å from one of the meta carbons in the benzene ring of Phe300. Simulated annealing omit maps also showed density in this region, suggesting that Phe300 is hydroxylated in the meta position, and subsequently hydrogen bonds to the main-chain carbonyl of Gln310 (Figure 2b). The ligand-free structure simulated annealing omit maps also clearly showed the hydroxylation of Phe300. Mass spectrometry analysis of the purified TyrOH shows a molecular weight which is 11−16 mass units too high for the known sequence, which is in accordance with the hydroxylation of a phenylalanine. No other protein modifications were observed in the *E. coli* expressed protein. The hydroxylated carbon of Phe300 is 3.9 Å from the C-4a carbon of the pterin, which is usually hydroxylated during enzyme turnover, and 6.6 Å away on a direct, unobstructed path from the iron. Both of these distances are very similar (4.0 and 6.9 Å) when taken from the other meta carbon of Phe300. Interestingly, the equivalent of Phe300 in PheOH (Phe254) does not appear to be hydroxylated and, in fact, does not have especially good density compared to other active site residues (H. Erlandsen, personal communication). The hydrogen bond which is formed as a result of the meta hydroxylation of Phe300 may serve to stabilize the position of this residue and allow for easier pterin binding to the active site.

Both rat TyrOH and human PheOH were expressed in *E. coli* strain BL21/DE3 for the published structural studies (*13*, *14*, *15*). This bacteria is known to contain pterin substrates for these enzymes (*24*) and dihydropteridine reductase for regenerating the pterin (*25*). Therefore, the required elements for enzyme turnover are present during expression, and the hydroxylation of Phe300 in TyrOH could be autocatalytic. Interestingly, PheOH shows no detectable activity with tyrosine as a substrate (*26*). This suggests that PheOH may strongly discriminate against hydroxylation at the meta position, thus preventing in vivo the unwanted diversion tyrosine. The presence of the meta hydroxylation of residue Phe300 only in TyrOH may be a result of this difference in specificity between the two enzymes.

Pterin Analogue Studies. A wide variety of pterin analogues have been examined as substrates of the aromatic amino acid hydroxylases (*1*, *3*). Substitutions of the dihydroxypropyl group are well tolerated, but do affect the kinetic parameters. As seen in Figure 4a, three hydrogen bonds link the dihydroxypropyl group to protein main-chain atoms or

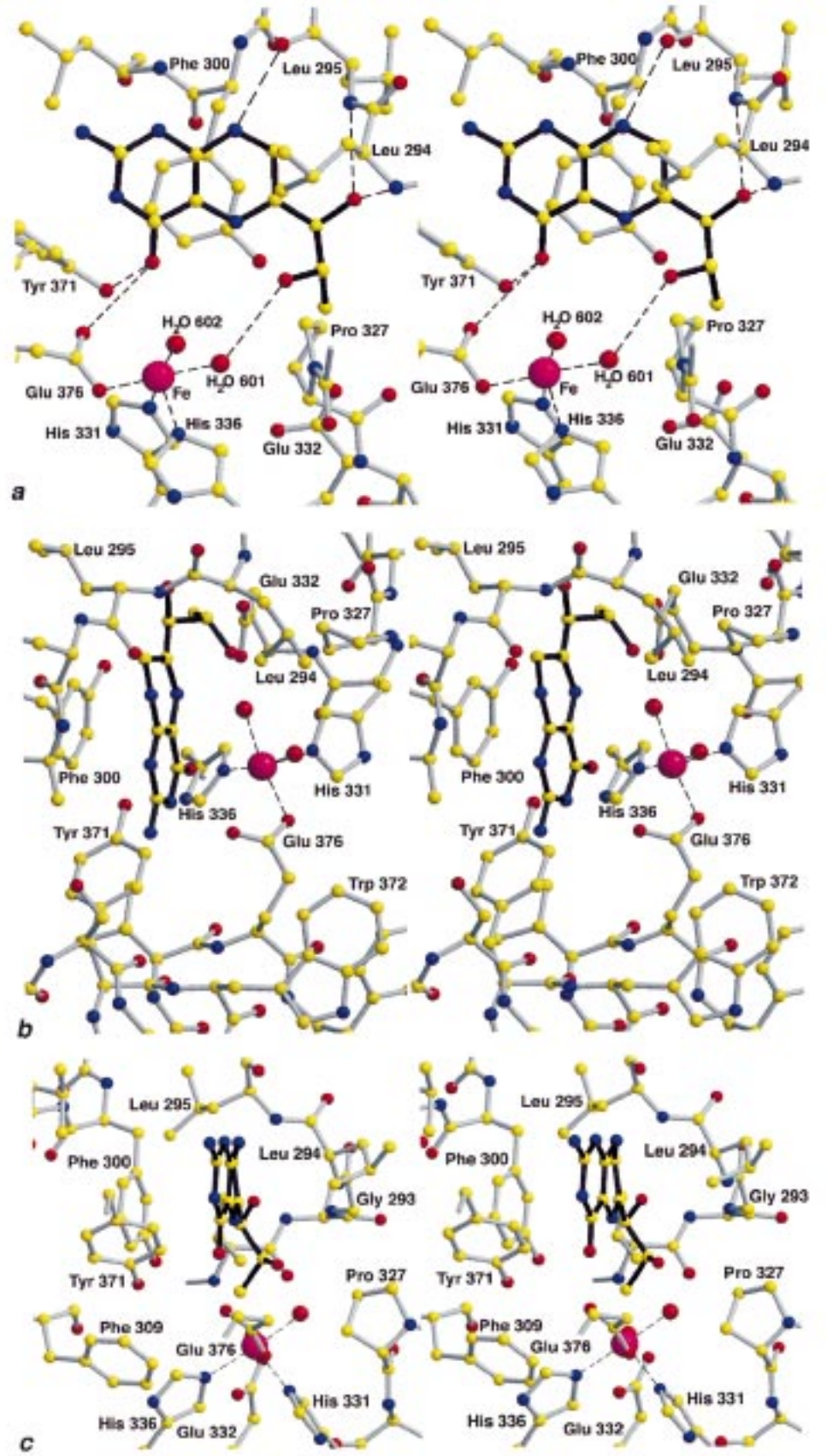

FIGURE 4: (a) A "front" stereoview of 7,8-dihydrobiopterin bound in the active site of TyrOH. Six hydrogen bonds from the pterin are shown as dashed lines. The iron coordination by two waters and three protein side chains is also shown by dashed lines. (b) A "top" stereoview of the pterin. Aromatic π-stacking can be seen between the pterin and the hydroxylated Phe300 side chain. (c) A "side" stereoview of the pterin. Possible oxygen binding residues are Phe309 (lower left) and Pro 327 (lower right).

one of the waters coordinated to the iron. The role of these hydrogen bonds is seen in TyrOH as a two to 4-fold increase in K_m for the pterin when 6-methyltetrahydropterin is substituted for tetrahydrobiopterin (*1*). Hydrophobic portions of the dihydroxypropyl-binding pocket are formed by Leu294, Pro327, and Val291 (Val291 is behind the pterin in Figure 4c). The hydrophobic aspect of this pocket may explain the 10-fold decrease in K_m when 6-phenyl and 6-cyclohexyl pterins are used as substrates (*27*). The lack of activity observed with a 6-carboxylate (*28*) may be due to an electrostatic repulsion by the nearby acidic residue Glu332.

The ability of 2,4,5-triamino-6-hydroxy-pyrimidine to function as a substrate for PheOH (*29*) has suggested a minimum configuration for the pterin. Enzyme activity with the pyrimidine suggests that positions 6 and 7 of the pterin ring are not required for activity, and these positions are among the furthest from the iron in the crystal structure (6.5 and 7.6 Å, respectively). The pyrimidine retains the hydrogen bonds seen from the pterin ring system at N-8 and the C-4 carbonyl (hydroxyl in the pyrimidine). The substitution of the carbonyl at C-4 with an amine was seen for the active substrate 6-methyl-2,4-diamino-tetrahydropterin (*28*), suggesting a nonspecific role for this substituent of the pterin which is 3.6 Å from the iron in the crystal structure. Substitution of the amine at position C-2 of the pterin with an oxygen or hydrogen has been shown to eliminate PheOH enzyme activity (*29*), although no direct contact of this substituent with the protein is seen in the crystal structure. A methyl-amine at this position is tolerated, but the dimethylamine is not (*30*).

A pterin analogue, 5-[(3-azido-6-nitrobenzylidene)amino]-2,6-diamino-4-pryimidinone (ANBADP), was used to probe the active site of PheOH by photoaffinity labeling (*31*). This probe was found to be a competitive inhibitor with respect to tetrahydrobiopterin and to label the enzyme with approximately a 1:1 stoichiometry. Tryptic digests showed that the label was primarily at Lys198, with some also at Lys194. These residues correspond to Ala245 and Lys 241 in TyrOH. The C_α of Lys241 is seen in the structure to be 18 Å from the iron, on the surface of the enzyme. Instead of binding to the active site, this pterin analogue may have bound to an aromatic patch just beneath the lysine, composed of PheOH residues Phe190, Tyr197, and Phe209.

Putative Amino Acid Substrate Binding Site. Kaufman has proposed that a not fully appreciated aspect of both PheOH and TyrOH is the effect of pterin variation on the K_m of the amino acid substrate (*1*). For example, the K_m of tyrosine is 10−20 times lower when tetrahydrobiopterin is used as cosubstrate, compared to using 6,7-dimethyltetrahydropterin. This observation, combined with the ordered binding of pterin before oxygen and tyrosine as observed for TyrOH (*8*), suggests that the pterin may itself form part of the binding surface for the tyrosine substrate. Further hints about the location of the amino acid binding site come from a comparison of the known sequences in the three types of aromatic amino acid hydroxylases. These comparisons have shown that TyrOH most likely diverged first from the common ancestral enzyme, with PheOH and TrpOH diverging more recently (*3*). However, the active-site residues of PheOH and TyrOH appear to be the most similar, as might be expected due to the similarity of their amino acid substrates. Two residues are strikingly different in TrpOH compared to the other two family members. Trp372 is conserved in all TyrOH and PheOH sequences, but is a much smaller tyrosine in TrpOH. Leu294 (in the pterin binding loop) is also conserved in all TyrOH and PheOH sequences, but is a larger tyrosine residue in TrpOH. These two differences in TrpOH may allow that enzyme to preferentially hydroxylate tryptophan. The position of these two residues relative to the pterin and iron can be seen in Figure 4b. The region bracketed by Leu294 at the top, the pterin to the left, Trp372 at the bottom, and the iron in the back may form the substrate-binding region.

Site-Specific Mutagenesis. A monoclonal anti-idiotype antibody has been generated which mimics the pterin molecule (*32*). The antibody binds to PheOH, but is prevented from binding when 6,7-dimethyl-7,8-dihydropterin is present. It also has been shown to bind to a diverse range of pterin-related enzymes, including dihydropteridine reductase and sepiapterin reductase. The monoclonal antibody was found to bind to a peptide corresponding to residues 310−336 of rat TyrOH, which was proposed to be the pterin-binding site. In the binary complex structure, Gln310 and Cys311 have C_αs which are less than 5 Å from the pterin, but their side chains point away from the active-site surface. Residues 312−326 form an extended loop which is completely buried in the interior of the enzyme. Pro327 forms part of the active site surface and is within 5 Å of the iron. In the complex, Cγ of Pro327 is 3.2 Å from the pterin hydroxyl at C-2′. Mutation of this residue to an alanine in PheOH or TyrOH results in an active enzyme which shows a small increase in the K_m for tetrahydrobiopterin, indicating that Pro327 is not required for pterin binding (*33*). Mutation of this residue to a longer, hydrophobic leucine side chain disrupts pterin binding as seen by a 20-fold increase in the K_m for tetrahydrobiopterin in TyrOH. In PheOH, this proline to leucine mutation results in an unchanged K_m for tetrahydrobiopterin, but causes a 20-fold increase in K_m for phenylalanine and a 100-fold decrease in specific activity.

The other residue in this region which has been examined by mutagenesis is Glu332. In the binary complex structure, Glu332 is 4.0 Å from the pterin hydroxyl C-2′ atom. Mutation of this residue to an alanine in TyrOH has little affect on enzyme activity or the K_m for tetrahydrobiopterin (*33*). This is not unexpected since 6-methyltetrahydropterin lacks a C-2′ hydroxyl but is only slightly inferior to tetrahydrobiopterin as a substrate for TyrOH (*1*). In contrast, mutation of the corresponding glutamate in PheOH (Glu286) results in a 70-fold increase in K_m for tetrahydrobiopterin (*34*). The greater effect of the Glu to Ala mutation in PheOH may correspond to the large difference in K_m for 6-methyltetrahydropterin compared to tetrahydrobiopterin in this enzyme [20−30-fold in PheOH; 2−4-fold in TyrOH (*1*)]. Thus, the role of this glutamate in binding the dihydroxypropyl portion of the pterin may be more important in PheOH than in TyrOH.

Spectroscopic Studies. EXAFS and Mössbauer spectroscopy of TyrOH have previously shown that there are no major changes in the first coordination shell of the iron upon addition of tetrahydrobiopterin (*35*). However, the iron center of both TyrOH (*6*) and PheOH (*7*) is known to be reduced to the active ferrous state by a reaction involving the oxidation of reduced pterins. Catechols, which have been

Table 1: Metal to Pterin Distances: Crystallographic vs NMR Data

		NMR measured (Å)		
protons	X-ray (Å)[a] BH_2	BH_2[b]	6-MPH_4[b]	3-MPH_4[b]
H-7 (R&S)	8.6	6.2 ± 1.1	4.5 ± 0.80	7.1 ± 1.4
H-1′	7.1	5.3 ± 1.0		
C-3′ H_3	5.8	6.4 ± 1.3		
H-6	6.6		3.8 ± 0.65	5.6 ± 1.0
CH_3 at C-6	6.8		5.3 ± 0.90	
CH_3 at N-3	5.5			7.0 ± 1.3
		NMR modeled (Å)		
nonprotons	X-ray (Å) BH_2	BH_2	6-MPH_4	3-MPH_4
C-4a	5.6	3.6−4.1	3.0−4.0	4.0−4.5
O-4	3.6	3.3−4.1		
N-5	5.4	3.3−3.8		

[a] For methyl groups, the distance of the central carbon is given. For other protons, estimated distances are given. [b] BH_2, 7,8-dihydrobiopterin; 6-MPH_4, 6-methyl-tetrahydropterin; 3-MPH_4, 3-methyl-tetrahydropterin.

shown by resonance Raman studies to directly coordinate the ferric iron of TyrOH (*36*), are competitive inhibitors versus the pterin but noncompetitive inhibitors versus the tyrosine substrate (*8*). Structural studies of catechols bound to PheOH have shown that the catechol- binding site spatially overlaps with the pterin-binding site found in this study (Erlandsen, personal communication). Taken together, these results suggest that the pterin binds in close proximity to the iron, but not coordinated to it. The crystal structure is in accordance with these results, with the carbonyl oxygen at position C-4 making the closest contact to the iron at a distance of 3.6 Å.

Proton NMR has been used by Martínez et al. to study the conformation of 6-methyl-tetrahydropterin (*37*), 7,8-dihydrobiopterin, and 3-methyl-tetrahydropterin (*38*) bound to the active site of TyrOH. In these studies, the active-site iron was replaced with cobalt and metal−proton distances were measured by the paramagnetic probe-T_1 method. From the measured distances, families of models were calculated to estimate the distance from the metal to pterin C-4a position which is hydroxylated during enzyme turnover. A comparison of the X-ray and NMR derived distances is presented in Table 1. The NMR measurements are generally in agreement with the crystal structure analysis, especially with regard to the metal being closest to the O-4, C-4a, and N-5 portion of the pterin. There is also agreement about the dihydroxypropyl group of the pterin being in a closely packed (as opposed to extended) conformation, such that the C-3′ methyl group is relatively close to the metal. The NMR models of bound 7,8-dihydrobiopterin show the conformation of the hydroxyls at C-1′ and C-2′ to have a dihedral angle of $\Theta = 75-83°$ and the crystal structure has a dihedral angle at this position of $\Theta = 120°$. From the crystal structure, one would expect the methyl group of 3-methyl-tetrahydropterin to be in steric conflict with Tyr371 and Glu376 of the enzyme. This conflict could cause the generally longer metal−pterin distances seen for the NMR measurements with 3-methyl-tetrahydropterin. Overall, as seen in the EXAFS and Mössbauer spectroscopy, the NMR data shows the pterin to be close to the metal but not coordinated to it.

The Hydroxylation Reaction. Recently, the reaction of oxygen in TyrOH has been examined by ^{18}O kinetic isotope effects (*11*). These experiments show a change in bond order of the oxygen in the rate-determining step, and a magnitude of the isotope effect indicating that the formation of an iron-dioxygen species is not rate determining. This result, in combination with previous studies, led the authors to suggest that a one electron transfer from the tetrahydrobiopterin to oxygen forms a superoxide anion as the first reactive intermediate. This radical pair would then couple to form a 4a-peroxytetrahydrobiopterin intermediate which may or may not interact with the iron (Scheme 1).

The position of the pterin relative to the active site iron as observed in the binary complex crystal structure easily accommodates the 4a-peroxytetrahydrobiopterin intermediate, with possible bridging to the iron, that has previously been proposed by several groups (see Scheme 1) (*3*, *9*−*12*). Pterin binding is seen to displace a water at 3.1 Å from the iron in TyrOH and could possibly displace one of the coordinated waters of PheOH (*14*). The resulting binary complex has a distance from the iron to the hydroxylated pterin C-4a carbon of 5.6 Å. Therefore, molecular oxygen could almost simultaneously interact with the ferrous iron and the C-4a position. The region in the structure between the iron and the C-4a carbon is buttressed by the completely conserved residues Phe309 and Pro327. The hydrophobic region formed by one of these two residues may promote oxygen binding (Figure 4c). Kinetic experiments show rapid equilibrium binding of oxygen (*8*), indicating weak binding of oxygen to the binary complex. Water 601 in this figure, which coordinates to the iron and is 5.1 Å from C-4a of the pterin, might be displaced during the hydroxylation reaction. Interestingly, Benkovic et al. (*39*) have determined the absolute configuration of the 4a-hydroxypterin product to have the oxygen pointing toward Phe309 as viewed in Figure 4c, which is the more buried side of the bound pterin.

This structure represents the first report of close interactions between pterin and iron in an enzyme active site. The proximity of the pterin to the iron can provide insight regarding the iron requirement of pterin-dependent monooxygenases compared to the metal-free catalysis of flavin-dependent monooxygenases (*40*). Tetrahydrobiopterin free in solution has a psuedo-first order autoxidation rate constant of approximately 10^{-6} s^{-1}, compared to productive turnover numbers of ~ 6 s^{-1} for PheOH and ~ 2 s^{-1} for TyrOH (*26*). In contrast, the reaction of flavins with oxygen is many orders of magnitude faster than pterin oxidation, and the reaction rates of flavoproteins range both above and below the autoxidation rate (*41*). Another difference with the flavoproteins, and possible role for the iron, is the ability of the aromatic amino hydroxylases to react with unactivated aromatic and aliphatic C−H substrates. Further studies of other pterin- and iron-dependent monooxygenases (eukaryotic glyceryl-ether monooxygenase (EC 1.14.16.5), bacterial anthranilate 3-monooxygenase (EC 1.14.16.3), and mandelate 4-monooxygenase (EC 1.14.16.6)) (*42*) should contribute to a better understanding of the pterin−iron interaction of the aromatic amino acid hydroxylases.

ACKNOWLEDGMENT

We thank M. Soltis and P. Kuhn for their help at beamline 7-1 at the Stanford Synchrotron Radiation Laboratory and T. Earnest at the Lawrence Berkeley National Laboratory

for providing computational facilities. We greatly appreciate valuable discussions on this manuscript with J. Klinman, W. Francisco, T. Flatmark, A. Martinez, and H. Erlandsen.

REFERENCES

1. Kaufman, S. (1995) *Adv. Enzymol. Relat. Areas Mol. Biol. 70*, 103−220.
2. Crane, B. R., Arvai, A. S., Ghosh, D. K., Wu, C., Getzoff, E. D., Stuehr, D. J., and Tainer, J. A. (1998) *Science 279*, 2121−2126.
3. Hufton, S. E., Jennings, I. G., and Cotton, R. G. H. (1995) *Biochem. J. 311*, 353−366.
4. Carr, R. T., Balasubramanian, S., Hawkins, P. C., and Benkovic, S. J. (1995) *Biochemistry 34*, 7525−7532.
5. Zhao, G., Xia, T., Song, J., and Jensen, R. A. (1994) *Proc. Natl. Acad. Sci. U.S.A. 91*, 1366−1370.
6. Ramsey, A. J., Hillas, P. J., and Fitzpatrick, P. F. (1996) *J. Biol. Chem. 271*, 24395−24400.
7. Wallick, D. E., Bloom, L. M., Gaffney, B. J., and Benkovic, S. J. (1984) *Biochemistry 23*, 1295−1302.
8. Marota, J. J., and Shiman, R. (1984) *Biochemistry 23*, 1303−1311.
9. Fitzpatrick, P. F. (1991) *Biochemistry 30*, 3658−3662.
10. Hillas, P. J., and Fitzpatrick, P. F. (1996) *Biochemistry 35*, 6969−6975.
11. Francisco, W. A., Tian, G., Fitzpatrick P. F., and Klinman J. P. (1998) *J. Am. Chem. Soc. 120*, 4057−4062.
12. Dix, T. A., Kuhn, D. M., and Benkovic, S. J. (1987) *Biochemistry 26*, 3354−3361.
13. Goodwill, K. E., Sabatier, C., Marks, C., Raag, R., Fitzpatrick, P. F., and Stevens, R. C. (1997) *Nat. Struct. Biol. 4*, 578−585.
14. Erlandsen, H., Fusetti, F., Martínez, A., Hough, E., Flatmark, T., and Stevens, R. C. (1997) *Nat. Struct. Biol. 4*, 995−1000.
15. Fusetti, F., Erlandsen, H., Flatmark, T., and Stevens, R. C. (1998) *J. Biol. Chem. 272*, 16962 (1998).
16. Martínez, A., Abeygunawardana, C., Haavik, J., Flatmark, T., Mildvan, A. S. (1993) *Biochemistry 32*, 6381−6390.
17. Otwinowski, Z., and Minor, W. (1996) *Methods Enzymol. 276*, 307−326.
18. *CCP4: A Suite of Programs for Protein Crystallography* (1979) SERC Daresbury Laboratory, Warrington WA4 4AD, U.K.
19. Adams, P. D., Pannu, N. S., Read, R. J., and Brünger, A. T. (1997) *Proc. Natl. Acad. Sci. U.S.A. 94*, 5018−5023.
20. Jones, T. A., Zou, J.-Y, Cowan, S. W., and Kjeldgaard, M. (1991) *Acta Crystallogr., A 47*, 110−119.
21. Laskowski, R. A., MacArthus, M. W., Moss, D. S., and Thornton, J. M. (1993) *J. Appl. Crystallogr. 26*, 283−291.
22. Hegg, E. L., and Que, L., Jr. (1997) *Eur. J. Biochem. 250*, 625−629.
23. McTigue, M. A., Davies, J. F., Kaufman, B. T., and Kraut, J. (1992) *Biochemistry 31*, 7264−7273.
24. Nixon, J. C. (1985) in *Folates and Pterins 2* (Blakley, R. L., and Benkovic, S. J., Eds.) pp 1−42, John Wiley & Sons, NY.
25. Vasudevan, S. G., Shaw, D. C., and Armarego, W. L. (1988) *Biochem J. 255*, 581−588.
26. Daubner, S. C., Hillas, P. J., and Fitzpatrick, P. F. (1997) *Biochemistry 36*, 11574−11582.
27. Bailey, S. W., Dillard, S. B., Thomas, K. B., and Ayling, J. E. (1989) *Biochemistry 28*, 494−504.
28. Ayling, J. E., Boehm, G. R., Textor, S. C., and Pirson, R. A. (1973) *Biochemistry 12*, 2045−2051.
29. Kaufman, S. (1979) *J. Biol. Chem. 254*, 5150−5154.
30. Kaufman, S. (1964) *J. Biol. Chem. 239*, 332−338.
31. Gibbs, B. S., and Benkovic, S. J. (1991) *Biochemistry 30*, 6795−6802.
32. Jennings, I. G., Kemp, B. E., and Cotton R. G. H. (1991) *Proc. Natl. Acad. Sci. U.S.A. 88*, 5734−5738.
33. Quinsey, N. S., Lenaghan, C. M., and Dickson, P. W. (1996) *J. Neurochem. 66*, 908−914.
34. Dickson, P. W., Jennings, I. G., and Cotton, R. G. (1994) *J. Biol. Chem. 269*, 20369−20375.
35. Meyer-Klaucke, W., Winkler, H., Schunemann, V., Trautwein, A. X., Nolting, H. F., and Haavik, J. (1996) *Eur. J. Biochem. 241*, 432−439.
36. Michaud-Soret, I., Andersson, K. K., Que, L., Jr., and Haavik, J. (1995) *Biochemistry 34*, 5504−5510.
37. Martínez, A., Abeygunawardana, C., Haavik, J., Flatmark, T., and Mildvan, A. S. (1993) *Adv. Exp. Med. Biol. 338*, 77−80.
38. Martínez, A., Vageli, O., Pfleiderer, W., and Flatmark, T. (1998) *Pteridines 9*, 44−52.
39. Dix, T. A., Bollag, G. E., Domanico, P. L., and Benkovic, S. J. (1985) *Biochemistry 24*, 2955−2958.
40. Massey, V., and Hemmerich, P. (1975) in *The Enzymes 12* (Boyer, P. D., Ed.) pp 191−252 Academic Press, NY.
41. Massey, V. (1994) *J. Biol. Chem. 269*, 22459−22462.
42. Kappock, T. J., and Caradonna, J. P. (1996) *Chem. Rev. 96*, 2659−2756.
43. Kraulis, P. J. (1991) *J. Appl. Crystallogr. 24*, 946−950.
44. Merritt, E. A., and Murphy, M. E. P. (1994) *Acta Crystallogr., Sect. D 50*, 869−873.
45. Esnouf, R. M. (1997) *J. Mol. Graphics 15*, 132−134.

BI981462G